

Nanocomposite of Conducting Polymer and Li Metal for Rechargeable High Energy Density Batteries

Lingyue Wang,^{||} Xiancheng Wang,^{||} Renming Zhan, Zhengxu Chen, Shuibin Tu, Chunhao Li, Xuerui Liu, Zhi Wei Seh, and Yongming Sun*



Cite This: <https://doi.org/10.1021/acsami.2c07917>



Read Online

ACCESS |



Metrics & More



Article Recommendations



Supporting Information

ABSTRACT: The structure and electrochemical performance of lithium (Li) metal degrade quickly owing to its hostless nature and high reactivity, hindering its practical application in rechargeable high energy density batteries. In order to enhance the electrochemical reversibility of metallic Li, we designed a Li/Li₂S-poly(acrylonitrile) (LSPAN) composite foil via a facile mechanical kneading approach using metallic Li and sulfurized poly(acrylonitrile) as the raw materials. The uniformly dispersed Li₂S-poly(acrylonitrile) (Li₂S-PAN) in a metallic Li matrix buffered the volume change on cycling, and its high Li ion conductivity enabled fast Li ion diffusion behavior of the composite electrode. As expected, the LSPAN electrode showed reduced voltage polarization, enhanced rate capability, and prolonged cycle life compared with the pure Li electrode. It exhibited stable cycling for 600 h with a symmetric cell configuration at 1 mA cm⁻² and 1 mA h cm⁻², far outperforming the pure metallic Li counterpart (400 h). Also, the LiCoO₂||LSPAN full cells with a cathode mass loading of ~16 mg cm⁻² worked stably for 100 cycles at 0.5 C with a high capacity retention of 96.5%, while the LiCoO₂||Li full cells quickly failed within only 50 cycles.

KEYWORDS: metallic Li, mechanical kneading, Li/Li₂S-poly(acrylonitrile) composite foil, stability, Li ion diffusion



1. INTRODUCTION

Li metal is considered as the ultimate anode candidate for rechargeable high energy density Li-based batteries owing to its high theoretical specific capacity (3.86 A h g⁻¹) and low reduction potential (-3.04 V).¹⁻⁴ Unfortunately, it is premature for practical application at the current stage due to several significant issues, including high reactivity and uncontrollable Li plating/stripping behavior due to its hostless nature.^{5,6} The random electrochemical Li deposition and its uneven dissolution behavior lead to the formation of loose structures and metallic Li dendrites on cycling.^{7,8} The high reactivity of Li causes severe side reactions, accompanied by a continuous increase in accessible surface area between metallic Li and the electrolyte during cycling, leading to accumulation of a resistive solid electrolyte interphase (SEI), consumption of the electrolyte, and increase in electrode thickness, and finally fast cell failure.⁹⁻¹¹

To solve the above problems, tremendous studies have been conducted, including electrolyte engineering,¹²⁻¹⁴ electrode-electrolyte interface design,¹⁵⁻¹⁷ and construction of the composite structure.¹⁸⁻²⁰ Among them, Li metal composite design has been probed as a promising approach to improve electrochemical performance by introducing functional components. For instance, the Li/reduced graphite oxide (RGO) composite possessed good structural stability due to the mechanical support of the RGO matrix. The RGO Li/graphite composite showed enhanced electrochemical reversibility via replacing the Li plating/stripping mechanism by the

conversion-deintercalation delithiation mechanism.²¹ The Li/Li₂₂Sn₅ composite showed significant advantages in rate capability due to the rich inner charge transport pathway of the electrode.^{22,23} Therefore, it is desirable to realize novel Li metal composites beyond that of the above inorganic components, which could bring new insights into understanding Li metal electrodes or significant advances.

Here, the potential of the Li-ion conducting polymer/Li metal composite is proposed and explored for advanced rechargeable Li metal batteries. Sulfurized poly(acrylonitrile) (SPAN) features abundant cross-linking polysulfide chains, which could spontaneously react with metallic Li to form Li₂S-PAN phases.^{24,25} With strong affinity with Li, a uniform and dense composite structure between metallic Li and Li₂S-PAN could be produced. Employing a facile mechanical kneading method, Li/Li₂S-PAN (LSPAN) composite foil was successfully fabricated using SPAN and metallic Li as the raw materials. The high Li ion conductivity of the uniformly embedded Li₂S-PAN phases ensures fast Li ion diffusion over the electrode and buffers the volume change on cycling, which support stable electrochemical cycling. As a result, the as-

Received: May 4, 2022

Accepted: August 2, 2022

obtained LSPAN electrode delivered extended cyclic life, reduced overpotential, and extraordinary rate capability. The LSPAN||LSPAN symmetric cells showed stable cycling for 600 h with a negligible overpotential increase at 1 mA cm^{-2} and 1 mA h cm^{-2} , while the Li||Li symmetric cells showed a sharp increase in overpotential after 400 h of cycling. Also, the LiCoO_2 ||LSPAN full cells with a high cathode mass loading of $\sim 16 \text{ mg cm}^{-2}$ exhibited a high capacity retention of 96.5% for 100 cycles at 0.5 C ($1 \text{ C} = 140 \text{ mA g}^{-1}$), far outperforming the LiCoO_2 ||Li cells that failed after only 50 cycles.

2. EXPERIMENTAL SECTION

2.1. Synthesis of SPAN. Commercial sulfur (S, AR 99.9%, Aladdin) and poly(acrylonitrile) (PAN, $M_w = 150,000$, Aladdin) were uniformly mixed (1.75:1 in weight) and sealed in a stainless steel container. The SPAN powder was obtained after thermal treatment at $350 \text{ }^\circ\text{C}$ for 10 h.

2.2. Synthesis of the LSPAN Composite Foil. The LSPAN composite foil was synthesized utilizing the reaction between SPAN and metallic Li via a facile mechanical kneading method. During the fabrication, a Li|SPAN|Li sandwich was first fabricated by spreading a certain amount of SPAN powders (5, 15, 20, 25, and 30 wt %, based on the weight of Li and SPAN composite) between two pieces of Li metal foils. Subsequently, repeated folding and calendaring processes were conducted in an Ar-filled glovebox. The SPAN and metallic Li reacted during the operation, and a uniform LSPAN composite was finally obtained.

2.3. Fabrication of LiCoO_2 and LiFePO_4 Cathodes. A slurry approach was adopted to fabricate the LiCoO_2 cathode consisting of 90 wt % active material, 5 wt % polyvinylidene fluoride (PVDF) binder, and 5 wt % carbon black. During the fabrication, the slurry was mixed uniformly and cast onto an Al foil. The LiCoO_2 cathodes were dried in air for 6 h at $60 \text{ }^\circ\text{C}$ and then rested in a vacuum oven for 12 h at $60 \text{ }^\circ\text{C}$. The operation for the fabrication of LiFePO_4 cathodes was similar. It consisted of 90 wt % active material, 5 wt % PVDF binder, and 5 wt % carbon black. The average active mass loadings of LiCoO_2 and LiFePO_4 electrodes were both $\sim 16 \text{ mg cm}^{-2}$.

2.4. Material Characterization. The compositions and morphologies of LSPAN composite foils were identified by X-ray photoelectron spectroscopy (XPS, AXIS-ULTRA DLD-600 W), X-ray diffraction (XRD, PANalytical B.V.), electron probe microanalysis (EPMA, Shimadzu EPMA-8050G), and field emission scanning electron microscopy (FESEM, Gemini SEM 300).

2.5. Electrochemical Measurements. A polypropylene membrane (Celgard 2500) was employed as the separator for coin cell assembly, and the electrolyte was 1 M LiPF_6 in ethylene carbonate/dimethyl carbonate/ethyl methyl carbonate (EC/DMC/EMC, 1:1:1 in volume) with the addition of 5 wt % fluoroethylene carbonate (FEC). Electrochemical impedance spectroscopy (EIS) and linear sweep voltammetry (LSV) measurements were recorded on a Biologic VMP3 and SP-50 workstation. EIS was conducted with the frequency range from 100 mHz to 100 kHz. LSV was conducted with a scan rate of 0.1 mV s^{-1} from -0.13 to 0.13 V .²⁶ Galvanostatic charge/discharge tests were measured on a Neware BTS-5 V battery test system. LSPAN||LSPAN and Li||Li symmetric cells were tested under 1 mA h cm^{-2} with different current densities. LiCoO_2 ||LSPAN and LiCoO_2 ||Li full cells were first charged/discharged at 0.1 C ($1 \text{ C} = 140 \text{ mA g}^{-1}$) for three activation cycles and then charged/discharged at 0.5 C in the cutoff voltage range from 2.8 to 4.3 V. LiFePO_4 ||LSPAN and LiFePO_4 ||Li full cells were cycled at 1 C with the cutoff voltage range from 2.5 to 4.2 V.

3. RESULTS AND DISCUSSION

Figure 1 schematically shows the morphology evolution of the LSPAN and pure Li electrodes with cycling. The uniform implantation of the conductive $\text{Li}_2\text{S-PAN}$ within metallic Li could help to homogenize Li ion flux and their fast transport

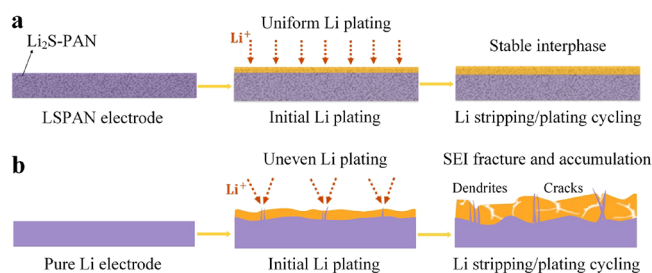


Figure 1. Schematic diagrams of electrochemical Li dissolution/deposition processes of (a) the LSPAN and (b) pure Li electrodes. Due to the uniform implantation of conductive $\text{Li}_2\text{S-PAN}$, uniform Li plating/stripping behavior takes place for the LSPAN electrode, featured by the formation of a stable SEI, and planar Li deposition, in comparison to the fast accumulation of inactive “dead Li” and SEI for the pure Li electrode.

on the LSPAN electrode, enabling planar Li plating with a stable SEI and thus high Li utilization (Figure 1a). In contrast, inactive “dead Li” and Li dendrites were observed on the pure Li electrode caused by inhomogeneous Li dissolution/deposition behavior, which eventually leads to fast electrode failure (Figure 1b).^{27,28}

The LSPAN composite foil was obtained using SPAN and metallic Li as the raw materials employing mechanical kneading operations, which is schematically shown in Figure 2a. Sulfur in SPAN is in the form of C–S, S–S bonds bonded to the conductive polymer backbone, and it can spontaneously react with metallic Li to produce $\text{Li}_2\text{S-PAN}$, which has a strong affinity with the Li substrate to form a dense structure.²⁹ The LSPAN composite foil showed a smooth and dense surface structure (Figure 2b) and good flexibility, supporting good mechanical stability (Figure 2c), which were beneficial for the subsequent materials processing and battery fabrication. To verify the formation of LSPAN composite foils, XRD measurement was conducted. The XRD pattern of the LSPAN composite foil showed three obvious peaks for Li_2S at ~ 27.0 , ~ 44.8 , and $\sim 65.2^\circ$ (2θ) besides the diffraction peaks for pure Li, and the bump at $\sim 25.0^\circ$ for the SPAN almost disappeared in the XRD pattern of the final product,³⁰ which suggested the conversion of SPAN to $\text{Li}_2\text{S-PAN}$ and formation of the LSPAN composite (Figure 2d). To further investigate the electronic structure and surface compositions of the LSPAN composite foil, XPS measurement was conducted. Different from the XPS spectra of the SPAN composite (Figure S1), new peaks were formed in the S 2p and Li 1s XPS spectra of the LSPAN composite (Figure 2e,f and Figure S2). Peaks at 161.88 and 163.03 eV in the high-resolution S 2p spectrum (Figure 2e) and a peak at 55.24 eV in the high-resolution Li 1s spectrum (Figure 2f) together suggested the formation of Li–S bonds,^{31,32} verifying the formation of the LSPAN composite foil. Besides, the peak at 54.66 eV in the high-resolution Li 1s spectrum (Figure 2f) suggested the presence of metallic Li besides $\text{Li}_2\text{S-PAN}$.³³ The elemental distribution of the LSPAN composite foil was investigated using EPMA. The elemental mapping images displayed the homogeneous distribution of the S element (Figure 2g), which supported the well-dispersed $\text{Li}_2\text{S-PAN}$ species in the metallic Li matrix. $\text{Li}_2\text{S-PAN}$ species were closely connected with metallic Li and formed a compact structure, which was favorable for forming a stable LSPAN composite and endowing fast and uniform Li ion diffusion over the electrode. With 25 wt % SPAN in the raw materials, the

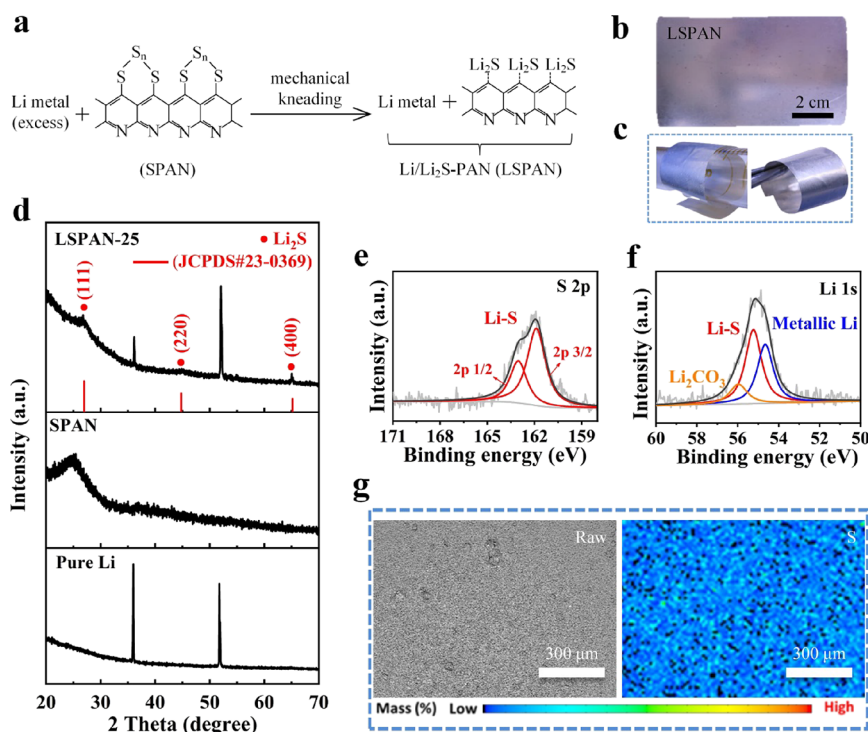


Figure 2. (a) Synthesis of the LSPAN composite foil. (b) Digital photo of the LSPAN electrode. (c) The curving test of the LSPAN composite foil. (d) XRD patterns of SPAN, LSPAN composite, and pure Li. High-resolution (e) S 2p and (f) Li 1s XPS spectra of the LSPAN composite foil. (g) Morphology and sulfur elemental mapping image of the LSPAN composite foil by EPMA.

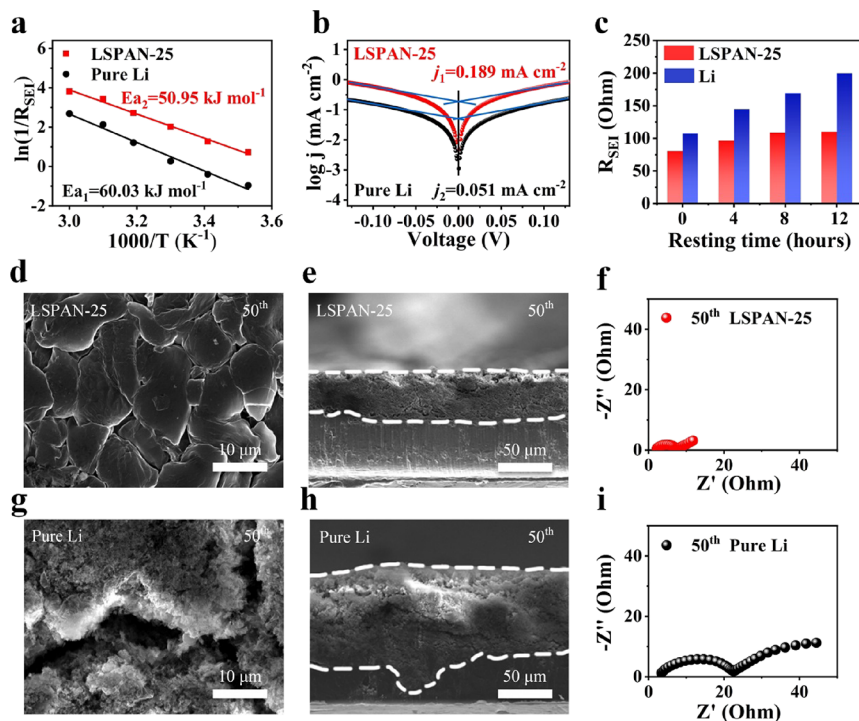


Figure 3. (a) Linear fitting of the R_{SEI} and temperature according to the relationship in the Arrhenius formula. (b) Tafel curves of LSPAN||LSPAN and Li||Li symmetric cells (c) Comparison of the fitted R_{SEI} values for the LSPAN and pure Li electrodes after resting for different times. SEM images of (d, e) the LSPAN electrode and (g, h) pure Li electrode after 50 cycles at 1 mA cm^{-2} and 1 mA h cm^{-2} . Nyquist plots for the (f) LSPAN||LSPAN and (i) Li||Li symmetric cells after 50 cycles at 1 mA cm^{-2} and 1 mA h cm^{-2} .

LSPAN composite foil displayed a satisfactory specific capacity of $\sim 2248 \text{ mA h g}^{-1}$ (Figure S3).

To understand the fast reaction kinetics of the LSPAN electrode, the activation energy (E_a) of Li ion diffusion through

the SEI at different temperatures was investigated through EIS measurement of the LSPAN||LSPAN and Li||Li symmetric cells (Figure S4a,b). The relationship between the interface impedance (R_{SEI}) and temperature is described by the

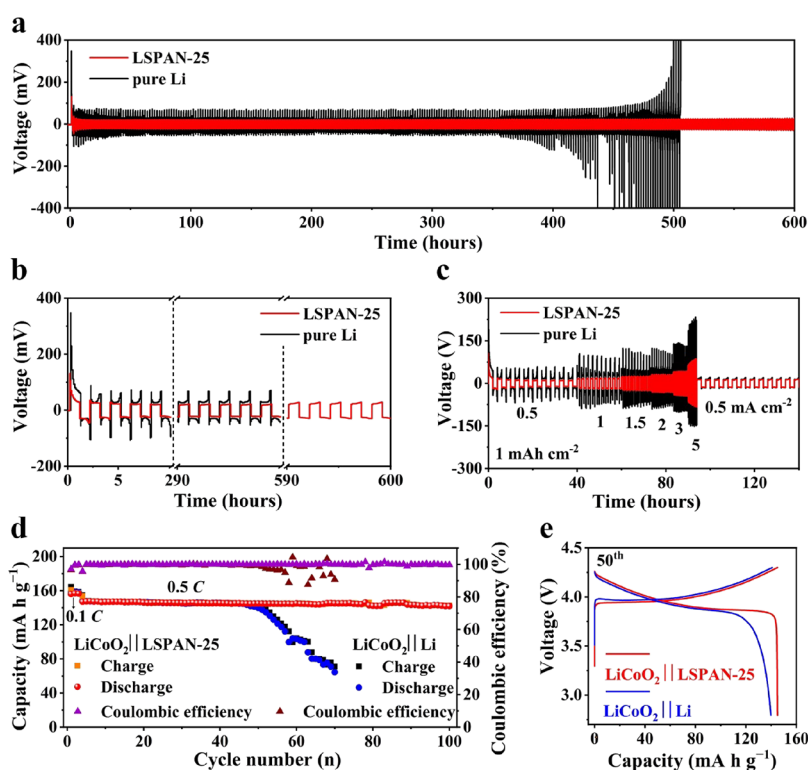


Figure 4. (a) Voltage profiles of the LSPAN||LSPAN and Li||Li symmetric cells cycling at 1 mA cm^{-2} and 1 mA h cm^{-2} and (b) the corresponding enlarged voltage profiles at different cycles. (c) Voltage profiles of the LSPAN||LSPAN and Li||Li symmetric cells cycling at different current densities of 0.5, 1, 1.5, 2, 3, and 5 mA cm^{-2} (10 cycles for each current density). (d) Cycling performance of LiCoO_2 ||LSPAN and LiCoO_2 ||Li full cells at 0.5 C and (e) their corresponding voltage profiles at the 50th cycle. Before long-term cycling, three activation cycles at 0.1 C were conducted. The negative/positive capacity (N/P) ratio of the full cells was 4.

Arrhenius formula $R_{\text{SEI}}^{-1} = A \exp(-E_a/RT)$.^{34–36} E_a for Li ion diffusion was obtained by linearly fitting $\ln(R_{\text{SEI}}^{-1})$ with T^{-1} (Figure 3a). The value of the E_a for Li ion diffusion of the LSPAN anode was lower than that of the pure Li anode (50.95 and $60.03 \text{ kJ mol}^{-1}$, respectively), suggesting improved Li ion diffusion behavior of the LSPAN electrode. The LSPAN electrode showed a higher exchange current density (0.189 mA cm^{-2}) than the pure Li counterpart (0.051 mA cm^{-2}) (Figure 3b), indicating its much faster Li ion transfer kinetics.³⁷ EIS measurements for the LSPAN||LSPAN and Li||Li symmetric cells after different resting times were conducted to compare the electrode interface stability in the organic electrolyte. The Nyquist plots after fitting with the equivalent circuit (Figure S4d) are shown in Figure S5, and the values of R_{SEI} are shown in Table S2. As illustrated in Figure 3c, the values of R_{SEI} of the LSPAN electrode were lower than that of the pure Li electrode, and it showed only a slight increase after resting (~ 109 and $\sim 110.2 \text{ } \Omega$ after 8 and 12 h of resting, respectively). In contrast, the pure Li electrode exhibited a notable increase in values of R_{SEI} after resting (~ 169.3 and $\sim 199.9 \text{ } \Omega$ after 8 and 12 h of resting, respectively). These results verified the fast interphase Li ion diffusion capability and good stability of the LSPAN electrode, which were beneficial for inhibiting the side reactions and prolonging the cyclic lifespan.

The morphology and structure of the LSPAN and pure Li electrodes with cycling were further investigated by SEM. The LSPAN composite foil exhibited a flat surface structure with chunky Li deposits after the initial Li plating at 1 mA cm^{-2} and 1 mA h cm^{-2} , indicating planar Li deposition behavior (Figure S6a,c). On the contrary, the pure Li electrode exhibited an uneven surface structure full of whiskery and dendritic Li

deposits after Li plating (Figure S6b,d). The uniform Li plating behavior of the LSPAN electrode could be attributed to the fast and homogeneous Li ion diffusion through the interface and was favorable for good cycling stability.³⁸ In addition, the surface of the LSPAN electrode remained uniform and compact after 50 cycles (Figure 3d and Figure S7a), which further indicated that the uniform implantation of $\text{Li}_2\text{S-PAN}$ phases within metallic Li could stabilize the interphase structure and regulate the deposition/dissolution behavior of Li on cycling. On the contrary, the loose surface structure of the pure Li electrode consisted of plenty of cracks (Figure 3g and Figure S7b).³⁹ Correspondingly, the cross-sectional SEM images showed a much thinner reaction layer of $\sim 40 \text{ } \mu\text{m}$ for the LSPAN electrode than for the pure Li electrode (over $80 \text{ } \mu\text{m}$). Such results suggest improved Li utilization and suppressed inactive Li accumulation of the LSPAN anode with cycling.⁴⁰

The Nyquist plots of the LSPAN||LSPAN and Li||Li symmetric cells after 50 cycles at 1 mA cm^{-2} and 1 mA h cm^{-2} are shown in Figure 3f,i. The R_{SEI} of the LSPAN electrode was lower than the pure Li electrode (~ 7 and $\sim 25 \text{ } \Omega$, respectively), again supporting the suppressed side reactions and inactive Li accumulation. The R_{SEI} of the LSPAN and pure Li electrodes were further compared after long-term cycling. The low value of R_{SEI} ($< 11 \text{ } \Omega$) was maintained after 100 cycles for the LSPAN electrode due to its stable electrode structure (Figure S8a). In sharp contrast, the R_{SEI} of the pure Li electrode increased quickly from ~ 25 to $\sim 75 \text{ } \Omega$ in 100 cycles due to the formation of a loose electrode structure, thick inactive Li layer, abundant Li dendrites, and fast consumption of the electrolyte on cycling (Figure S8b).⁴¹

To investigate the electrochemical cycling stability and rate capability of the LSPAN electrode, galvanostatic Li plating/stripping cycling tests were conducted for the LSPAN||LSPAN and Li||Li symmetric cells. The thicknesses of the LSPAN and pure Li electrodes for symmetric cells were both 100 μm (Figure S9a,b). Due to the fast Li ion diffusion capability, the LSPAN electrode exhibited smooth voltage profiles with lower overpotential (~ 20 mV) in comparison to that of the pure Li electrode (~ 27 mV) and displayed a longer cyclic lifespan of above 600 h compared to 400 h for the pure Li electrode (Figure 4a). The enlarged voltage profiles in Figure 4b showed that the voltage profiles of the LSPAN electrode remained flat with little overpotential increase even after 300 cycles, indicating its good electrochemical stability during long-term Li plating/stripping cycling. On the contrary, the pure Li symmetric cell showed large voltage fluctuation and high overpotential after 350 h of cycling, and it showed a rapid increase in overpotential and failed after 400 h of cycling owing to its poor Li ion diffusion ability and the unstable interface structure.⁴² The rate behaviors of the LSPAN and Li symmetric cells were tested under 1 mA h cm^{-2} at various current densities (Figure 4c). The pure Li symmetric cells showed large voltage fluctuation, indicating its inferior structural stability, while the LSPAN symmetric cells remained stable voltage profiles with only slight change in overpotential under different current densities, supporting the high stability of the LSPAN electrode.^{43,44}

We further studied its electrochemical performance in full cells paired with LiCoO_2 cathodes. The thicknesses of the LSPAN and pure Li electrodes for full cells were 80 and 50 μm , respectively (Figure S9c,d), corresponding to the total areal capacity of 10 mA h cm^{-2} . With a cathode mass loading of ~ 16 mg cm^{-2} , the as-fabricated LiCoO_2 ||LSPAN cells exhibited stable potential curves and displayed a high capacity retention of 96.5% for 100 cycles at 0.5 C, revealing the excellent cycling stability of the LSPAN electrode (Figure 4d,e and Figure S10). In contrast, rapid capacity decay occurred for LiCoO_2 ||Li full cells after only 50 cycles owing to the fast failure of the pure Li anode. The electrodes after cycling were measured by SEM and XRD. The cathodes of the LiCoO_2 ||LSPAN and LiCoO_2 ||Li full cells after 70 cycles both exhibited an intact structure at the electrode and particle levels and showed four typical peaks for LiCoO_2 at ~ 19.0 , ~ 37.4 , ~ 45.3 , and $\sim 59.6^\circ$ (JCPDS#16-0427), which were similar to the fresh ones (Figures S11 and S12), indicating the stable phase structure of LiCoO_2 cathodes during cycling. As shown in Figures S13 and S14, the LSPAN electrode remained a stable structure after 70 cycles. In contrast, loose structures with abundant cracks were observed for the pristine Li electrode after cycling, indicating the advantages of LSPAN in enhancing the electrode stability and prolonging the lifespan of cells. The C-rate capability of the LiCoO_2 ||LSPAN and LiCoO_2 ||Li cells were also tested at 0.1 C, 0.2 C, 0.5 C, 1 C, 2 C, and 4 C. As shown in Figure S15, the cell using LSPAN anode delivered higher specific capacity than that using the pure Li anode. The capacity retention of the LiCoO_2 ||LSPAN cell was 65.8% at 2 C (104.5 mA h g^{-1}), much higher than 29.3% (45.7 mA h g^{-1}) for the LiCoO_2 ||Li cell, suggesting the advancement of the LSPAN electrode in realizing high rate capability of cells. Also, the LiFePO_4 ||LSPAN full cells showed stable cycling for 150 cycles at 1 C (1 C = 160 mA g^{-1}) with a high capacity retention of 96.4% under a high cathode mass loading of ~ 16 mg cm^{-2} (Figures

S16 and 17), while the LiFePO_4 ||Li counterpart decayed quickly.

LSPAN composites with different initial SPAN contents (x wt %, $x = 5, 15, 20, 30$, based on the entire composite electrode) were fabricated, and their electrochemical performances were compared. All LSPAN- x symmetric cells delivered better electrochemical cycling stability than the pure Li symmetric cells (at 1 mA cm^{-2} and 1 mA h cm^{-2} , Figures S18–S21). The high Li utilization and excellent cycling stability of the LSPAN composite foil make it a promising choice for Li metal batteries.

4. CONCLUSIONS

In summary, a LSPAN composite foil was designed utilizing the spontaneous reaction between SPAN and metallic Li via a facile mechanical kneading method. The high Li ion conductivity of Li_2S -PAN phases ensured fast Li ion diffusion over the electrode, and its reduced reactivity suppressed the side reactions between the electrode and the organic electrolyte. The uniform implantation of Li_2S -PAN phases within the entire electrode could also work as a framework to support stable Li deposition/dissolution. As a result, the LSPAN electrode possessed significantly extended cyclic lifespan and better rate capability in comparison to the pure Li electrode. Also, the LiCoO_2 ||LSPAN full cells with a cathode mass loading of ~ 16 mg cm^{-2} exhibited stable cycling, low overpotential, and high capacity retention of 96.5% at 0.5 C for 100 cycles. This work provides a general mechanical kneading method for introducing conducting polymer in metallic Li and improving its electrochemical performance, which can be extended to other metal anodes as well.

■ ASSOCIATED CONTENT

Supporting Information

The Supporting Information is available free of charge at <https://pubs.acs.org/doi/10.1021/acsami.2c07917>.

Additional figures showing the XPS spectra, Nyquist plots, tables of the values of fitted R_{SEI} , SEM images, digital photos, electrochemical performance, and XRD patterns (PDF)

■ AUTHOR INFORMATION

Corresponding Author

Yongming Sun – Wuhan National Laboratory for Optoelectronics, Huazhong University of Science and Technology, Wuhan 430074, China; orcid.org/0000-0001-8528-525X; Email: yongmingsun@hust.edu.cn

Authors

Lingyue Wang – Wuhan National Laboratory for Optoelectronics, Huazhong University of Science and Technology, Wuhan 430074, China

Xiancheng Wang – Wuhan National Laboratory for Optoelectronics, Huazhong University of Science and Technology, Wuhan 430074, China

Renming Zhan – Wuhan National Laboratory for Optoelectronics, Huazhong University of Science and Technology, Wuhan 430074, China

Zhengxu Chen – Wuhan National Laboratory for Optoelectronics, Huazhong University of Science and Technology, Wuhan 430074, China

Shuibin Tu – Wuhan National Laboratory for Optoelectronics, Huazhong University of Science and Technology, Wuhan 430074, China

Chunhao Li – Wuhan National Laboratory for Optoelectronics, Huazhong University of Science and Technology, Wuhan 430074, China

Xuerui Liu – Wuhan National Laboratory for Optoelectronics, Huazhong University of Science and Technology, Wuhan 430074, China

Zhi Wei Seh – Institute of Materials Research and Engineering, Agency for Science, Technology and Research (A*STAR), Singapore 138634, Singapore; orcid.org/0000-0003-0953-567X

Complete contact information is available at:
<https://pubs.acs.org/10.1021/acsami.2c07917>

Author Contributions

^{||}L.W. and X.W. contributed equally to this work.

Notes

The authors declare no competing financial interest.

ACKNOWLEDGMENTS

The work is supported by the National Natural Science Foundation of China (52072137). The authors sincerely thank the Analytical and Testing Center of Huazhong University of Science and Technology for providing the facilities to conduct the characterization. Z.W.S. acknowledges the Singapore National Research Foundation (NRF-NRFF2017-04) and Agency for Science, Technology and Research (Central Research Fund Award).

REFERENCES

- (1) Zhang, X.; Yang, Y.; Zhou, Z. Towards Practical Lithium-Metal Anodes. *Chem. Soc. Rev.* **2020**, *49*, 3040–3071.
- (2) Liu, J.; Bao, Z.; Cui, Y.; Dufek, E. J.; Goodenough, J. B.; Khalifah, P.; Li, Q.; Liaw, B. Y.; Liu, P.; Manthiram, A.; Meng, Y. S.; Subramanian, V. R.; Toney, M. F.; Viswanathan, V. V.; Whittingham, M. S.; Xiao, J.; Xu, W.; Yang, J.; Yang, X.-Q.; Zhang, J.-G. Pathways for Practical High-Energy Long-Cycling Lithium Metal Batteries. *Nat. Energy* **2019**, *4*, 180–186.
- (3) Fang, C.; Li, J.; Zhang, M.; Zhang, Y.; Yang, F.; Lee, J. Z.; Lee, M.-H.; Alvarado, J.; Schroeder, M. A.; Yang, Y.; Lu, B.; Williams, N.; Ceja, M.; Yang, L.; Cai, M.; Gu, J.; Xu, K.; Wang, X.; Meng, Y. S. Quantifying Inactive Lithium in Lithium Metal Batteries. *Nature* **2019**, *572*, 511–515.
- (4) Cheng, Y.; Chen, J.; Chen, Y.; Ke, X.; Li, J.; Yang, Y.; Shi, Z. Lithium Host: Advanced Architecture Components for Lithium Metal Anode. *Energy Storage Mater.* **2021**, *38*, 276–298.
- (5) Albertus, P.; Babinec, S.; Litzelman, S.; Newman, A. Status and Challenges in Enabling the Lithium Metal Electrode for High-Energy and Low-Cost Rechargeable Batteries. *Nat. Energy* **2018**, *3*, 16–21.
- (6) Ding, J.-F.; Xu, R.; Yan, C.; Li, B.-Q.; Yuan, H.; Huang, J.-Q. A Review on the Failure and Regulation of Solid Electrolyte Interphase in Lithium Batteries. *J. Energy Chem.* **2021**, *59*, 306–319.
- (7) Yan, C.; Cheng, X.-B.; Tian, Y.; Chen, X.; Zhang, X.-Q.; Li, W.-J.; Huang, J.-Q.; Zhang, Q. Dual-Layered Film Protected Lithium Metal Anode to Enable Dendrite-Free Lithium Deposition. *Adv. Mater.* **2018**, *30*, 1707629.
- (8) Xiao, J. How Lithium Dendrites Form in Liquid Batteries. *Science* **2019**, *366*, 426–427.
- (9) Kim Mun, S.; Deepika; Lee Seung, H.; Kim, M.-S.; Ryu, J.-H.; Lee, K.-R.; Archer Lynden, A.; Cho Won, I. Enabling Reversible Redox Reactions in Electrochemical Cells Using Protected Lial Intermetallics as Lithium Metal Anodes. *Sci. Adv.* **2019**, *5*, eaax5587.
- (10) Wang, Y.; Wang, Z.; Lei, D.; Lv, W.; Zhao, Q.; Ni, B.; Liu, Y.; Li, B.; Kang, F.; He, Y.-B. Spherical Li Deposited inside 3D Cu Skeleton as Anode with Ultrastable Performance. *ACS Appl. Mater. Interfaces* **2018**, *10*, 20244–20249.
- (11) Horstmann, B.; Shi, J.; Amine, R.; Werres, M.; He, X.; Jia, H.; Hausen, F.; Cekic-Laskovic, I.; Wiemers-Meyer, S.; Lopez, J. J. E.; Science, E. Strategies Towards Enabling Lithium Metal in Batteries: Interphases and Electrodes. *Energy Environ. Sci.* **2021**, *14*, 5289–5314.
- (12) Pang, Q.; Shyamsunder, A.; Narayanan, B.; Kwok, C. Y.; Curtiss, L. A.; Nazar, L. F. Tuning the Electrolyte Network Structure to Invoke Quasi-Solid State Sulfur Conversion and Suppress Lithium Dendrite Formation in Li-S Batteries. *Nat. Energy* **2018**, *3*, 783–791.
- (13) Zhang, H.; Eshetu, G. G.; Judez, X.; Li, C.; Rodriguez-Martinez, L. M.; Armand, M. Electrolyte Additives for Lithium Metal Anodes and Rechargeable Lithium Metal Batteries: Progress and Perspectives. *Angew. Chem., Int. Ed.* **2018**, *57*, 15002–15027.
- (14) Tan, Y.-H.; Lu, G.-X.; Zheng, J.-H.; Zhou, F.; Chen, M.; Ma, T.; Lu, L.-L.; Song, Y.-H.; Guan, Y.; Wang, J.; Liang, Z.; Xu, W.-S.; Zhang, Y.; Tao, X.; Yao, H.-B. Lithium Fluoride in Electrolyte for Stable and Safe Lithium-Metal Batteries. *Adv. Mater.* **2021**, *33*, 2102134.
- (15) Tu, Z.; Choudhury, S.; Zachman, M. J.; Wei, S.; Zhang, K.; Kourkoutis, L. F.; Archer, L. A. Fast Ion Transport at Solid-Solid Interfaces in Hybrid Battery Anodes. *Nat. Energy* **2018**, *3*, 310–316.
- (16) Li, C. C.; Zhang, X.-S.; Zhu, Y.-H.; Zhang, Y.; Xin, S.; Wan, L.-J.; Guo, Y.-G. Modulating the Lithiophilicity at Electrode/Electrolyte Interface for High-Energy Li-Metal Batteries. *Energy Mater.* **2021**, *1*, 100017.
- (17) Liu, Y.; Tao, X.; Wang, Y.; Jiang, C.; Ma, C.; Sheng, O.; Lu, G.; Lou Xiong, W. Self-Assembled Monolayers Direct a LiF-Rich Interphase toward Long-Life Lithium Metal Batteries. *Science* **2022**, *375*, 739–745.
- (18) Li, S.; Liu, Q.; Zhou, J.; Pan, T.; Gao, L.; Zhang, W.; Fan, L.; Lu, Y. Hierarchical Co₃O₄ Nanofiber-Carbon Sheet Skeleton with Superior Na/Li-Philic Property Enabling Highly Stable Alkali Metal Batteries. *Adv. Funct. Mater.* **2019**, *29*, 1808847.
- (19) Zhao, Y.; Li, G.; Gao, Y.; Wang, D.; Huang, Q.; Wang, D. Stable Li Metal Anode by a Hybrid Lithium Polysulfidophosphate/Polymer Cross-Linking Film. *ACS Energy Lett.* **2019**, *4*, 1271–1278.
- (20) Niu, C.; Pan, H.; Xu, W.; Xiao, J.; Zhang, J.-G.; Luo, L.; Wang, C.; Mei, D.; Meng, J.; Wang, X.; Liu, Z.; Mai, L.; Liu, J. Self-Smoothing Anode for Achieving High-Energy Lithium Metal Batteries under Realistic Conditions. *Nat. Nanotechnol.* **2019**, *14*, 594–601.
- (21) Wang, H.; Cao, X.; Gu, H.; Liu, Y.; Li, Y.; Zhang, Z.; Huang, W.; Wang, H.; Wang, J.; Xu, W.; Zhang, J.-G.; Cui, Y. Improving Lithium Metal Composite Anodes with Seeding and Pillaring Effects of Silicon Nanoparticles. *ACS Nano* **2020**, *14*, 4601–4608.
- (22) Wan, M.; Kang, S.; Wang, L.; Lee, H.-W.; Zheng, G. W.; Cui, Y.; Sun, Y. Mechanical Rolling Formation of Interpenetrated Lithium Metal/Lithium Tin Alloy Foil for Ultrahigh-Rate Battery Anode. *Nat. Commun.* **2020**, *11*, 829.
- (23) Wang, X.; He, Y.; Tu, S.; Fu, L.; Chen, Z.; Liu, S.; Cai, Z.; Wang, L.; He, X.; Sun, Y. Li Plating on Alloy with Superior Electro-Mechanical Stability for High Energy Density Anode-Free Batteries. *Energy Storage Mater.* **2022**, *49*, 135–143.
- (24) Yang, H.; Chen, J.; Yang, J.; Wang, J. Prospect of S@Ppan Cathode Materials for Rechargeable Lithium Batteries. *Angew. Chem.* **2019**, *132*, 7374–7386.
- (25) Wang, X.; Qian, Y.; Wang, L.; Yang, H.; Li, H.; Zhao, Y.; Liu, T. Sulfurized Polyacrylonitrile Cathodes with High Compatibility in Both Ether and Carbonate Electrolytes for Ultrastable Lithium-Sulfur Batteries. *Adv. Funct. Mater.* **2019**, *29*, 1902929.
- (26) Piao, Z.; Xiao, P.; Luo, R.; Ma, J.; Gao, R.; Li, C.; Tan, J.; Yu, K.; Zhou, G.; Cheng, H.-M. Constructing a Stable Interface Layer by Tailoring Solvation Chemistry in Carbonate Electrolytes for High-Performance Lithium-Metal Batteries. *Adv. Mater.* **2022**, *34*, 2108400.
- (27) Wang, X.; Zeng, W.; Hong, L.; Xu, W.; Yang, H.; Wang, F.; Duan, H.; Tang, M.; Jiang, H. Stress-Driven Lithium Dendrite

Growth Mechanism and Dendrite Mitigation by Electroplating on Soft Substrates. *Nat. Energy* **2018**, *3*, 227–235.

(28) Bai, P.; Guo, J.; Wang, M.; Kushima, A.; Su, L.; Li, J.; Brushett, F. R.; Bazant, M. Z. Interactions between Lithium Growths and Nanoporous Ceramic Separators. *Joule* **2018**, *2*, 2434–2449.

(29) Jiang, Z.; Guo, H.-J.; Zeng, Z.; Han, Z.; Hu, W.; Wen, R.; Xie, J. Reconfiguring Organosulfur Cathode by Over-Lithiation to Enable Ultrathick Lithium Metal Anode toward Practical Lithium-Sulfur Batteries. *ACS Nano* **2020**, *14*, 13784–13793.

(30) Zhao, C.-X.; Chen, W.-J.; Zhao, M.; Song, Y.-W.; Liu, J.-N.; Li, B.-Q.; Yuan, T.; Chen, C.-M.; Zhang, Q.; Huang, J.-Q. Redox Mediator Assists Electron Transfer in Lithium-Sulfur Batteries with Sulfurized Polyacrylonitrile Cathodes. *EcoMat* **2021**, *3*, No. e12066.

(31) Wang, Z.; Qi, F.; Yin, L.; Shi, Y.; Sun, C.; An, B.; Cheng, H.-M.; Li, F. An Anion-Tuned Solid Electrolyte Interphase with Fast Ion Transfer Kinetics for Stable Lithium Anodes. *Adv. Energy Mater.* **2020**, *10*, 1903843.

(32) Zhao, Q.; Utomo, N. W.; Kocen, A. L.; Jin, S.; Deng, Y.; Zhu, V. X.; Moganty, S.; Coates, G. W.; Archer, L. A. Upgrading Carbonate Electrolytes for Ultra-Stable Practical Lithium Metal Batteries. *Am. Chem. Soc. Div. Polym. Chem. Prepr.* **2022**, *134*, No. e202116214.

(33) Chen, C.; Liang, Q.; Wang, G.; Liu, D.; Xiong, X. Grain-Boundary-Rich Artificial Sei Layer for High-Rate Lithium Metal Anodes. *Adv. Funct. Mater.* **2022**, *32*, 2107249.

(34) Ouyang, Y.; Guo, Y.; Li, D.; Wei, Y.; Zhai, T.; Li, H. Single Additive with Dual Functional-Ions for Stabilizing Lithium Anodes. *ACS Appl. Mater. Interfaces* **2019**, *11*, 11360–11368.

(35) Zhai, P.; Liu, L.; Wei, Y.; Zuo, J.; Yang, Z.; Chen, Q.; Zhao, F.; Zhang, X.; Gong, Y. Self-Healing Nucleation Seeds Induced Long-Term Dendrite-Free Lithium Metal Anode. *Nano Lett.* **2021**, *21*, 7715–7723.

(36) Yao, Y.-X.; Chen, X.; Yan, C.; Zhang, X.-Q.; Cai, W.-L.; Huang, J.-Q.; Zhang, Q. Regulating Interfacial Chemistry in Lithium-Ion Batteries by a Weakly Solvating Electrolyte. *Angew. Chem., Int. Ed.* **2021**, *60*, 4090–4097.

(37) Meng, J.; Chu, F.; Hu, J.; Li, C. Liquid Polydimethylsiloxane Grafting to Enable Dendrite-Free Li Plating for Highly Reversible Li-Metal Batteries. *Adv. Funct. Mater.* **2019**, *29*, 1902220.

(38) Kim, M. S.; Zhang, Z.; Rudnicki, P. E.; Yu, Z.; Wang, J.; Wang, H.; Oyakhire, S. T.; Chen, Y.; Kim, S. C.; Zhang, W.; Boyle, D. T.; Kong, X.; Xu, R.; Huang, Z.; Huang, W.; Bent, S. F.; Wang, L.-W.; Qin, J.; Bao, Z.; Cui, Y. Suspension Electrolyte with Modified Li⁺ Solvation Environment for Lithium Metal Batteries. *Nat. Mater.* **2022**, *21*, 445–454.

(39) Qin, L.; Wu, Y.; Shen, M.; Song, B.; Li, Y.; Sun, S.; Zhang, H.; Liu, C.; Chen, J. Straining Copper Foils to Regulate the Nucleation of Lithium for Stable Lithium Metal Anode. *Energy Storage Mater.* **2022**, *44*, 278–284.

(40) Hou, L.-P.; Yao, L.-Y.; Bi, C.-X.; Xie, J.; Li, B.-Q.; Huang, J.-Q.; Zhang, X.-Q. High-Valence Sulfur-Containing Species in Solid Electrolyte Interphase Stabilizes Lithium Metal Anodes in Lithium-Sulfur Batteries. *J. Energy Chem.* **2022**, *68*, 300–305.

(41) Lu, Z.; Li, W.; Long, Y.; Liang, J.; Liang, Q.; Wu, S.; Tao, Y.; Weng, Z.; Lv, W.; Yang, Q.-H. Constructing a High-Strength Solid Electrolyte Layer by in Vivo Alloying with Aluminum for an Ultrahigh-Rate Lithium Metal Anode. *Adv. Funct. Mater.* **2020**, *30*, 1907343.

(42) Xu, P.; Hu, X.; Liu, X.; Lin, X.; Fan, X.; Cui, X.; Sun, C.; Wu, Q.; Lian, X.; Yuan, R.; Zheng, M.; Dong, Q. A Lithium-Metal Anode with Ultra-High Areal Capacity (50 mA h cm⁻²) by Gridding Lithium Plating/Stripping. *Energy Storage Mater.* **2021**, *38*, 190–199.

(43) Ye, S.; Wang, L.; Liu, F.; Shi, P.; Wang, H.; Wu, X.; Yu, Y. g-C₃N₄ Derivative Artificial Organic/Inorganic Composite Solid Electrolyte Interphase Layer for Stable Lithium Metal Anode. *Adv. Energy Mater.* **2020**, *10*, 2002647.

(44) Jin, C.; Liu, T.; Sheng, O.; Li, M.; Liu, T.; Yuan, Y.; Nai, J.; Ju, Z.; Zhang, W.; Liu, Y.; Wang, Y.; Lin, Z.; Lu, J.; Tao, X. Rejuvenating Dead Lithium Supply in Lithium Metal Anodes by Iodine Redox. *Nat. Energy* **2021**, *6*, 378–387.